**IOP**science

**IOP**science

 🔍    Journals ▼    Books    Publishing Support    👤 Login ▼

PAPER

# Carbon dots derived from frankincense soot for ratiometric and colorimetric detection of lead (II)

Varsha Lisa John[1] iD, Fasila P M[2] iD, Chaithra K P[1] iD and Vinod T P[1] iD

vinod.tp@christuniversity.in

[1] Department of Chemistry, CHRIST (Deemed to be University), Bangalore 560029, India

[2] Department of Chemistry, Sir Syed College, Taliparamba, Kannur, Kerala 670142, India

Varsha Lisa John iD https://orcid.org/0000-0002-3843-4686

Fasila P M iD https://orcid.org/0000-0002-2613-1610

Chaithra K P iD https://orcid.org/0000-0002-0518-7578

Vinod T P iD https://orcid.org/0000-0001-5815-5230

🔴 Check for updates

Method: Double-anonymous
Revisions: 2
Screened for originality? No

Buy this article in print

🔊 Journal RSS

🔔 Sign up for new issue notifications

## Abstract

We report a simple one-pot hydrothermal synthesis of carbon dots from frankincense soot. Carbon dots prepared from frankincense (FI-CDs) have narrow size distribution with an average size of 1.80 nm. FI-CDs emit intense blue fluorescence without additional surface functionalization or modification. A negative surface charge was observed for FI-CDs, indicating the abundance of epoxy, carboxylic acid, and hydroxyl functionalities that accounts for their stability. A theoretical investigation of the FI-CDs attached to oxygen-rich functional groups is incorporated in this study. The characteristics of FI-CDs signify arm-chair orientation, which is confirmed by comparing the indirect bandgap of FI-CDs with the bandgap obtained from Tauc plots. Also, we demonstrate that the FI-CDs are promising fluoroprobes for the ratiometric detection of $Pb^{2+}$ ions (detection limit of 0.12 $\mu$M). The addition of $Pb^{2+}$ to FI-CD solution quenched the fluorescence intensity, which is observable under illumination by UV light LED chips. We demonstrate a smartphone-assisted quantification of the fluorescence intensity change providing an efficient strategy for the colorimetric sensing of $Pb^{2+}$ in real-life samples.

Export citation and abstract          BibTeX          RIS

## Access this article

The computer you are using is not registered by an institution with a subscription to this article. Please choose one of the options below.

### Login

Access through your institution

IOPscience login

Find out more about journal subscriptions at your site.

## Purchase from

Article Galaxy
CCC RightFind

Purchase this article from our trusted document delivery partners.

## Rent from



This article is available from DeepDyve.

## Make a recommendation

To gain access to this content, please complete the Recommendation Form and we will follow up with your librarian or Institution on your behalf.

For corporate researchers we can also follow up directly with your R&D manager, or the information management contact at your company. Institutional subscribers have access to the current volume, plus a 10-year back file (where available).

## You may also like

### JOURNAL ARTICLES

Ascorbic Acid Nano-Dots with ROS Scavenging Properties for High Contrast Fluorescence Imaging

A Novel Electrochemical Sensor Based on Carbon Dots-Nafion Composite Modified Bismuth Film Electrode for Simultaneous Determination of $Cd^{2+}$ and $Pb^{2+}$

Heteroatom-Doping for Carbon Dots: An Efficient Strategy to Improve Their Optoelectronic Properties

Application of functionalized carbon dots in detection, diagnostic, disease treatment, and desalination: a review

A Novel Electrochemical Sensor Based on Carbon Dots-Nafion Composite Modified Bismuth Film Electrode for Simultaneous Determination of $Cd^{2+}$ and $Pb^{2+}$

A Facile Microwave-Assisted Synthesis of Carbon Dots and Their Application as Sensitizers in Nanocrystalline $TiO_2$ Solar Cells

# IOPSCIENCE

# IOP PUBLISHING

# PUBLISHING SUPPORT

Journals

Copyright 2024 IOP Publishing

Authors

Books

Terms and Conditions

Reviewers

IOP Conference Series

Disclaimer

Conference Organisers

About IOPscience

Privacy and Cookie Policy

Contact Us

Developing countries access

IOP Publishing open access policy

Accessibility

**IOP**

Research article

# A DFT study to unravel the fluorescence mechanisms of APTES-modified carbon dots

Varsha Lisa John [a], Fasila P.M. [b], Vinod T.P. [a] ⚲ ✉

- [a] Department of Chemistry, CHRIST (Deemed to be University), Bangalore, Karnataka 560029, India
- [b] Department of Chemistry, Sir Syed College, affiliated to Kannur University, Kannur, Kerala 670142, India

(?) What do these dates mean?

[ 🔴 Check for updates ]

Show less ∧

≡ Outline      ⊷ Share    ⟩⟩ Cite

Get rights and content ↗

## Abstract

Surface passivation is a well-established method for modifying carbon dots (CDs), intended to improve their properties. We present a theoretical study employing density functional theory (DFT) and time-dependent-DFT (TD-DFT) to explain the photoluminescence (PL) mechanism of amine-modified carbon dots (CD-$NH_2$) [CDs modified with (3-Aminopropyl) triethoxy silane (APTES)] considering their local geometry at the terminal ends; the zig-zag (CD$_{ZZ}$-$NH_2$) and armchair (CD$_{AC}$-$NH_2$) structural orientations. The experimental evidence from our previous report suggests that the amine groups were tethered on the surface of CDs through a Si-O bond realized by the silane coupling reaction between the ethoxy group of APTES and the hydroxyl group of the CDs. The effect of pH in tweaking the PL of these systems is scrutinized in the

present study. The influence of pH and structure on the bandgap of CD-NH$_2$ is demonstrated by analyzing the difference in HOMO-LUMO energies, the density of states (DoS) spectra, and electrostatic potentials (ESP).

## Graphical Abstract
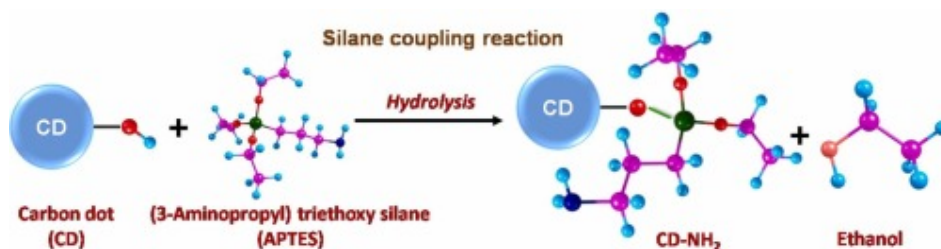
## Keywords

Carbon dots; TD-DFT; Hydrogen bonding; Silane coupling reaction; APTES modification; Photoluminescence mechanism; Electrostatic potential; The density of states

## 1. Introduction

Attempts to develop modification strategies for carbon dots (CDs) have evolved since discovering these particles [1], [2]. Apart from being zero-dimensional and having sizes upto 10nm, CDs are chemically inert, water-soluble, biocompatible, resilient to photobleaching, less toxic, easy to synthesize, and can be modified using simple methods [3], [4], [5], [6], [7], [8], [9] . Routes to modify CDs can be broadly classified into four major categories [10]; (i) surface functionalization/passivation [2], [11], [12], (ii) heteroatom doping [13], [14], (iii) composite material blending [15], [16], and (iv) core-shell architecture [17], [18]. These methods are intended to reform the CDs for particular applications by altering their photophysical properties [19], [20]. Surface passivation/functionalization, realized by incorporating functionalities such as -OH, -NH$_2$ on the surface of CDs, is popular due to the hassle-free methods of synthesis (comparing other routes) [21].

Koga et al. in 2011 introduced an in-situ modification technique suitable for functionalizing paper substrates [22], and Feng et al. in 2013 reported the synthesis of CDs from paper precursors [23]. The above results inspired synthesizing CDs from amine-modified paper precursors (CD-NH$_2$) by introducing a novel surface modification strategy [24]. Amine modification was realized by immersing paper substrates in an alcoholic solution of (3-

Aminopropyl) triethoxy silane (APTES) [22]. APTES, a versatile coupling agent, acts as a molecular bridge that attaches organic moieties (with its silanol groups) onto an inorganic substrate [25]. The binding of APTES on inorganic substrate happens through the silanol groups, while the $-NH_2$ groups are free to involve in further covalent derivatization [26]. With paper precursors, the ethoxy group of APTES and the $-OH$ group of the cellulose moieties on paper generate an O-Si bond on CDs (Fig. 1). This tethers $-NH_2$ functionality on the surface of CDs through a silane-coupling reaction [26], [27]. The major disadvantage of CD-NH$_2$ was the low quantum yield (QY), around 2%. Structural orientation (armchair/zig-zag), pH etc., are major contributing factors to CDs' photoluminescence (PL) [10], [28], [29]. Analyzing the PL mechanism employing theoretical calculations helps to devise new surface modification techniques and to redesign the existing modification strategies.
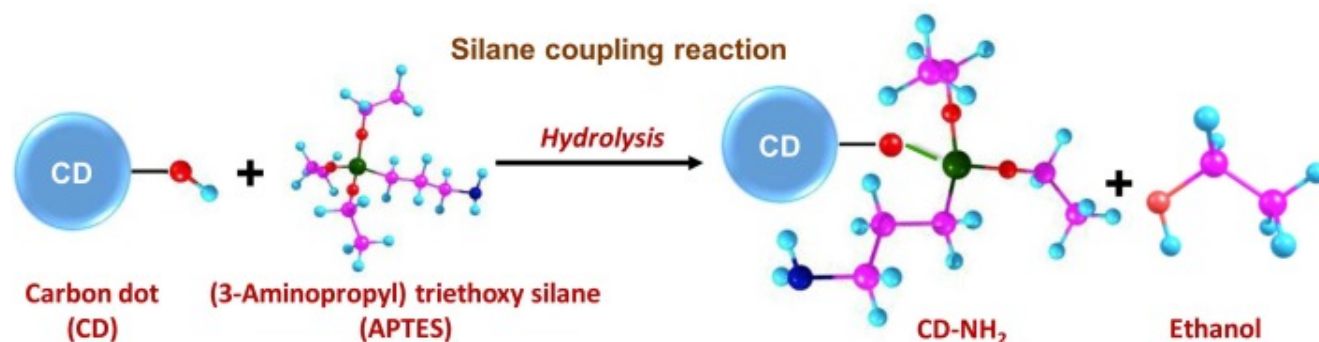


Download: Download high-res image (165KB)

Download: Download full-size image

Fig. 1. Schematic representation of the formation of Si-O bond when CDs are passivated with APTES via silane coupling reaction ( ●-O, ●-Si, ●-C, ●-N, ●-H).

This work is designed to unravel the PL mechanism using computational methods based on DFT/TD-DFT. The role of amine functionalities (present in the form of APTES) in tweaking the PL properties and the effect of pH on these amine-modified CDs are analyzed theoretically. The previous reports on the effect of $-OH$ moieties in tuning the bandgap of CDs helped the theoretical design of CDs discussed in the current study [21]. The details on the relative sizes of the CDs obtained from experimental results helped design the specific CDs that are the first of their kind [21], [24]. The CDs after APTES treatment (CD-NH$_2$) are compared with those before modification. The structural orientations of CDs play a pivotal role in tuning the PL characteristics; CD-NH$_2$s are designed to possess zig-zag/armchair (CD$_{ZZ}$-NH$_2$/CD$_{AC}$-NH$_2$) orientations at their edges. The sizes and structural orientations of CD-NH$_2$ are optimized per the above discussion. Since pH is a decisive factor in tuning the photophysical properties of CD-NH$_2$, the role of pH in tweaking the PL characteristics of CD-NH$_2$ is deliberated with the aid of orbital analysis (HOMO-LUMO), simulations of the density of states (DoS) spectra, UV spectra, structural analysis from IR spectra, Raman spectra, and XRD analysis. The article includes the experimental validation of the insights obtained from the DFT/TD-DFT calculations.

## 2. Computational methodology

The structures of CDs relevant to the study were optimized with Gaussian 09 program package [30]. CDs carrying Oxygen-containing functional groups have been optimized and compared with their corresponding graphitic layer previously [21]. The conductor-like polarizable continuum (CPCM) model was utilized to optimize all the structures with the solvent effects of water [31]. Gauss View 5.0 [32] and Chemcraft [33] were the visualization tools. The optimized method and basis set. [34] for simulating CDs were B3LYP [35], [36] and 6–31 G(d) [37]. The computational tools that helped the investigation of the photophysical properties of the CDs were orbital (HOMO-LUMO) analysis, molecular electrostatic potential (MEP), the density of states (DoS) spectra, UV–visible spectra, and natural bond orbital (NBO) [38] analysis. The density of states (DoS) spectra were obtained from the GaussSum program package [39]. The APTES-modified systems were subjected to a change of pH, and the effect of acids/bases on the –OH and –$NH_2$ groups, which would alter the charge and multiplicity of the system, were analyzed. Computational tools such as NBO and nuclear magnetic resonance (NMR) studies have helped validate the hydrogen bonds (HB) [40]. Calculations of chemical shielding (CS) tensors were performed on the CDs' optimized structures. The CS calculations were based on the gauge-independent atomic orbital (GIAO) theory [41], [42]. CS tensors help to understand the magnetic shielding effect induced due to the valence electrons around the nucleus of an atom. The principal components of a CS tensor are defined as $\sigma_{33} > \sigma_{22} > \sigma_{11}$. The isotropic CS tensor ($\sigma_{iso}$) is defined as $\sigma_{iso} = \left(\frac{\sigma_{33}+\sigma_{22}+\sigma_{11}}{3}\right)$.

## 3. Results and discussion

PL emission of CDs depends on various factors such as size, local geometry at the terminal ends (armchair/zig-zag structural orientation), surface defects, pH, ionic strength, excitation wavelength, aggregation etc. [10]. The major disadvantage of APTES-modified CDs synthesized from paper precursors was their low QY [24]. Here we investigate theoretical aspects of improving PL intensity with the structural orientation of CDs and variation in pH.

CDs synthesized from paper precursors contain abundant –OH moieties on their surface [23], [24]. Such an understanding led to the design of armchair/zig-zag oriented CDs ($CD_{AC}$/$CD_{ZZ}$) before modifying with APTES (Fig. 2). The zero-point vibrational energies ($E_{ZPV}$) of $CD_{AC}$ and $CD_{ZZ}$ are − 70,380.14 eV and − 72,813.79 eV, respectively (Fig. 3). The role of hydrogen bonding (HB) can't be neglected, as the structural orientation of $CD_{AC}$ favours intramolecular HB. The striking difference of 2433.65 eV between the zero-point vibrational energies of $CD_{AC}$ and $CD_{ZZ}$ is due to the intramolecular HB interactions in $CD_{AC}$. The spatial orientation of –OH groups of $CD_{AC}$ is favourable for intramolecular HB (O----H-C), which restricts the chances for intermolecular HB, unlike in the case of $CD_{ZZ}$. R. A. Klein confirms the ability of a force field to 'detect' HB by the summation of van der Waals (VDW) atomic radii [43]. VDW atomic radii are part of the parametrization to decide if the donor-acceptor (Oxygen-Hydrogen) atoms are close enough to form HBs. The –OH functionalities of $CD_{AC}$ and $CD_{ZZ}$ engage in intermolecular HB in the solvent, water. The -C-H---O bond distance in the case of $CD_{AC}$ is obtained within the range of 1.80 Å - 1.92 Å, shorter than the sum of VDW radii of Oxygen and Hydrogen atoms by 2.72 Å [43]. Based on Jeffrey's classification, bond lengths of HBs less than 2.20 Å are regarded as

strong bonds [44], [45], [46], [47]. Since the geometrical parametrization with VDW overestimates the separation between donor and acceptor that results in HBs, superior alternatives such as NBO and NMR studies must be sorted to investigate HBs.
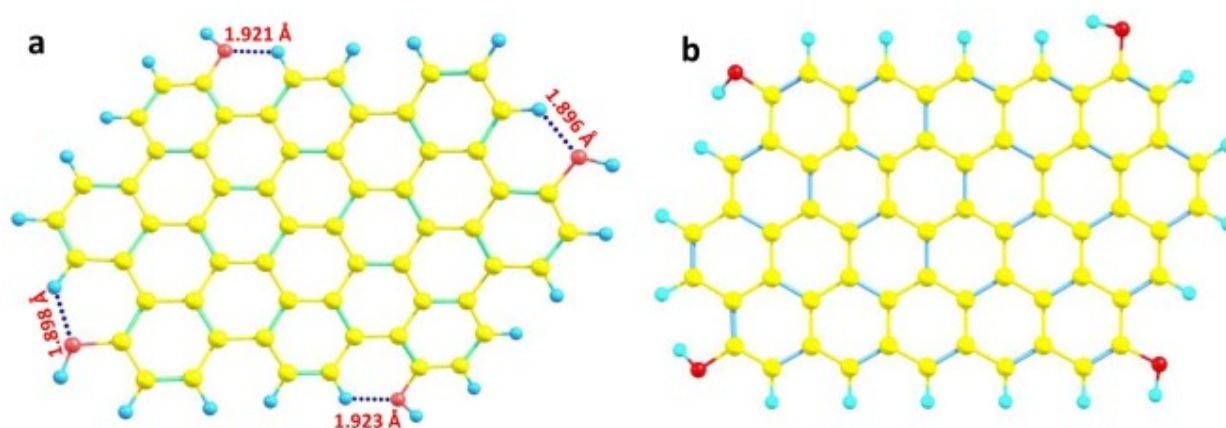


Download: Download high-res image (180KB)

Download: Download full-size image

Fig. 2. Optimized structures of (a) $CD_{AC}$ and (b) $CD_{ZZ}$. Display of HB interaction in $CD_{AC}$ (● -O, ● -C, ● -H).
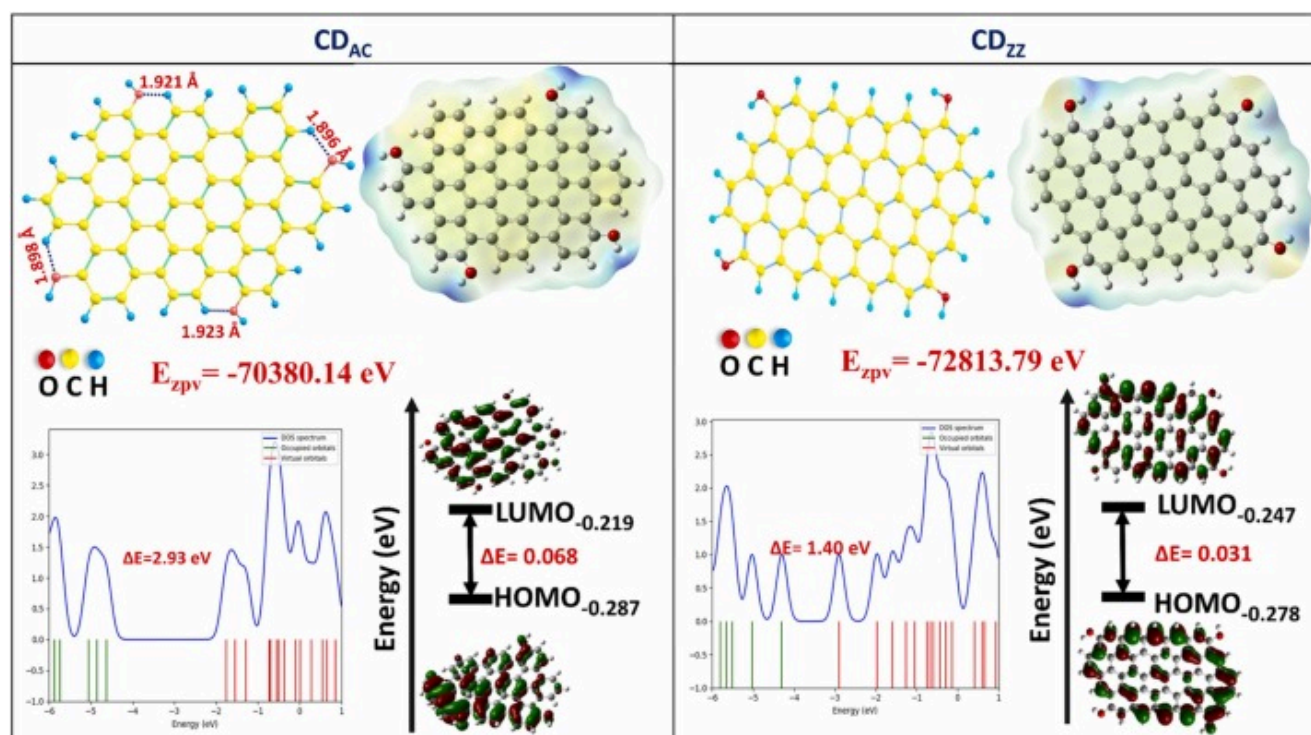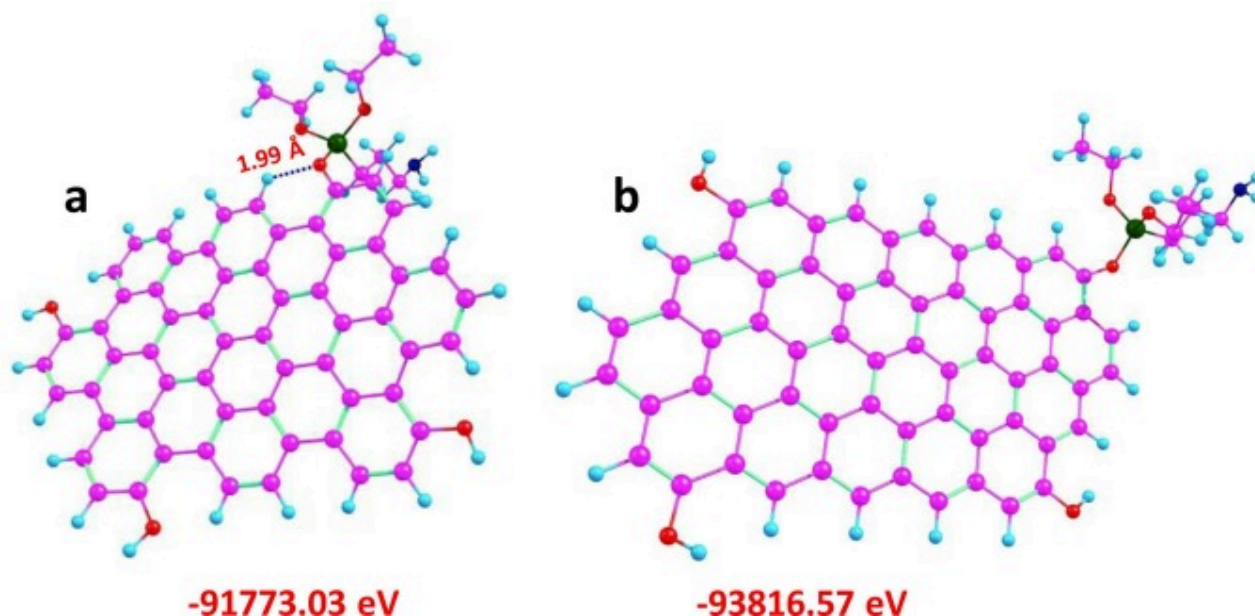


Download: Download high-res image (454KB)

Download: Download full-size image

Fig. 3. Comparison of the structure and emission characteristics of armchair and zig-zag oriented CDs before surface modification with APTES. The bandgap obtained from both DoS spectra and HOMO-LUMO energy levels are provided.

NBO analysis considers localized bonds and lone pairs as the basic unit of a molecular structure, comparable to the Lewis theory of covalent bonding and the Pauling-Slater-Coulson [48], [49], [50] theory of bond hybridization and polarization [51], [52]. The intramolecular HB interactions in $CD_{AC}$ (O----H-C) can be attributed to the delocalization of electrons from the lone pair of the donor atom Oxygen ($n_O$) to the unoccupied anti-bonding orbital of C-H ($\sigma^*_{CH}$) [40]. Such attractive interactions between the $n_O$ and $\sigma^*_{CH}$ give rise to the second-order perturbation energies, E(2), that can characterize the strength of HB [52]. In the case of $CD_{AC}$, E(2) correlates well with the O----H lengths of HBs (Table S1, Supplementary material). The electron delocalization is more as the HB gets closer. NMR analysis in association with geometry parametrization and NBO helps to explain hydrogen bonding in $CD_{AC}$. After enlisting the CS tensors of $^{13}C$ and $^{17}O$ (Table S1 and S2, Supplementary material), a blatant correlation of $\sigma_{iso}$ to the length of HBs has been revealed. The short bond lengths indicate that the HBs are strong, and the electrons concentrated around Oxygen atoms undergo the maximum effect of shielding. As the HB weakens, the deshielding of electrons causes downfield shifts.

The molecular electrostatic potential (MEP) diagrams help to identify the electrophilic sites in a molecular entity. The red colour in the MEP diagrams of Fig. 2 refers to the regions of minimum electrostatic potential (i.e., the abundance of electrons), suggesting that the –OH groups can facilitate further modification of $CD_{AC}$ and $CD_{ZZ}$ by forming covalent bonds [21]. The blue colour indicates the regions of maximum electrostatic potential and acts the opposite. The energy gap ($\Delta E$) obtained from the orbital analysis explains that zig-zag orientation lowers the bandgap more than armchair. In the HOMO-LUMO diagrams of $CD_{AC}$, the orbitals concentrate largely towards the basal plane. $CD_{ZZ}$'s uniform distribution of orbitals towards the edges has a lower energy gap than $CD_{AC}$. The non-bonding edge states created at the edges of $CD_{ZZ}$ explain the reason for the orbital distribution at their edges [53]. Such non-bonding edge states dominate the origin of electronic, magnetic and chemical activities of $CD_{ZZ}$. These non-bonding edge states are absent in $CD_{AC}$. The bandgap from the DoS spectra of $CD_{AC}$ and $CD_{ZZ}$ follows a similar trend. A comparison of the features mentioned above of $CD_{AC}$ and $CD_{ZZ}$ with their corresponding graphitic layers is carried out in the previous reports of our group [21].

Introducing APTES through a novel synthetic method described in the previous reports yielded $CD_{AC}$-$NH_2$ and $CD_{ZZ}$-$NH_2$, indicating the amine modification on armchair and zig-zag oriented CDs, respectively [24]. Modification attained via APTES treatment helped stabilize $CD_{AC}$-$NH_2$ and $CD_{ZZ}$-$NH_2$ by lowering $E_{ZPV}$ (Fig. 4). The length of the O-Si bond (formed due to silane coupling reaction and confirmed by NBO analysis) of $CD_{AC}$-$NH_2$ and $CD_{ZZ}$-$NH_2$ is 1.67 Å and 1.68 Å, respectively agrees with the experimentally observed value of 1.68 Å [54]. The C-N bond length within the APTES moiety observed in $CD_{AC}$-$NH_2$ and $CD_{ZZ}$-$NH_2$ (confirmed via NBO analysis) is 1.47 Å and 1.48 Å, respectively, which correlates with the experimental value of 1.47 Å [55].
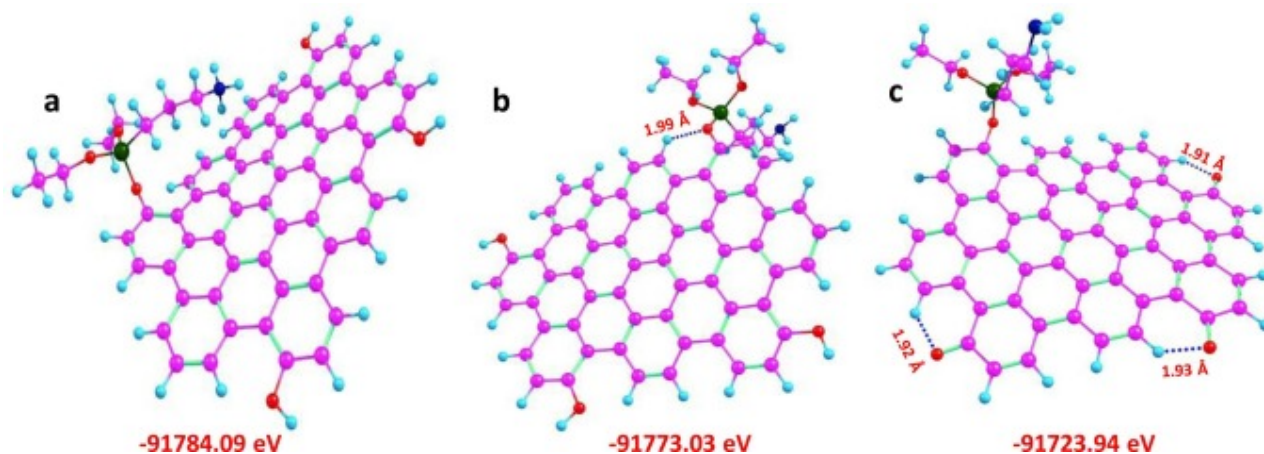
Download: Download high-res image (263KB)

Download: Download full-size image

Fig. 4. Optimized structures and $E_{ZPV}$ of (a) $CD_{AC}$–$NH_2$ and (b) $CD_{ZZ}$–$NH_2$. The colours of atoms present in the structure are O- ⬤, N- ⬤, Si- ⬤, C- ⬤, and H- ⬤. The $CD_{ZZ}$–$NH_2$ is stable due to its lowest $E_{ZPV}$.

---

$CD_{AC}$–$NH_2$ and $CD_{ZZ}$–$NH_2$ were subjected to a change of pH, and the effect of acids/bases on the -OH and -$NH_2$ groups, which would alter the charge and multiplicity of the system, was analyzed. Fig. 5 gives an account of the behaviour of $CD_{AC}$-$NH_2$ in the presence of acids and bases. When pH< 7, -OH groups on $CD_{AC}$-$NH_2$ are unaffected, and the -$NH_2$ groups are protonated, forming quaternary ammonium complexes. The C-N bond length is determined to be 1.52 Å, indicating the formation of the quaternary ammonium complex. Comparing the $E_{ZPV}$ when pH > 7 and pH = 7, $CD_{AC}$-$NH_2$ is energetically stable when pH < 7 as it lacks intramolecular HB. The chances of intramolecular HB are restricted due to the constraints of geometry parameters, such as the distance of HB and the alignment of –OH bonds to different planes. In neutral conditions, APTES modification resulted in minimizing the HB interactions limiting to just one after validating with geometry parameters and tools like NBO (Table S3, Supplementary material). When pH > 7, the –OH groups are oxidized to ketones. There are high chances of intramolecular HB in $CD_{AC}$-$NH_2$ when pH > 7 with the O-H bond distances ranging from 1.91–1.93 Å. The electron delocalization indicated by E(2) improves when the HB strengthens (Table S3, Supplementary material). The CS tensors of $^{13}$C and $^{17}$O throw light to correlate the HB strength to the shielding of electrons (Table S4, Supplementary material) as in the case of $CD_{AC}$.
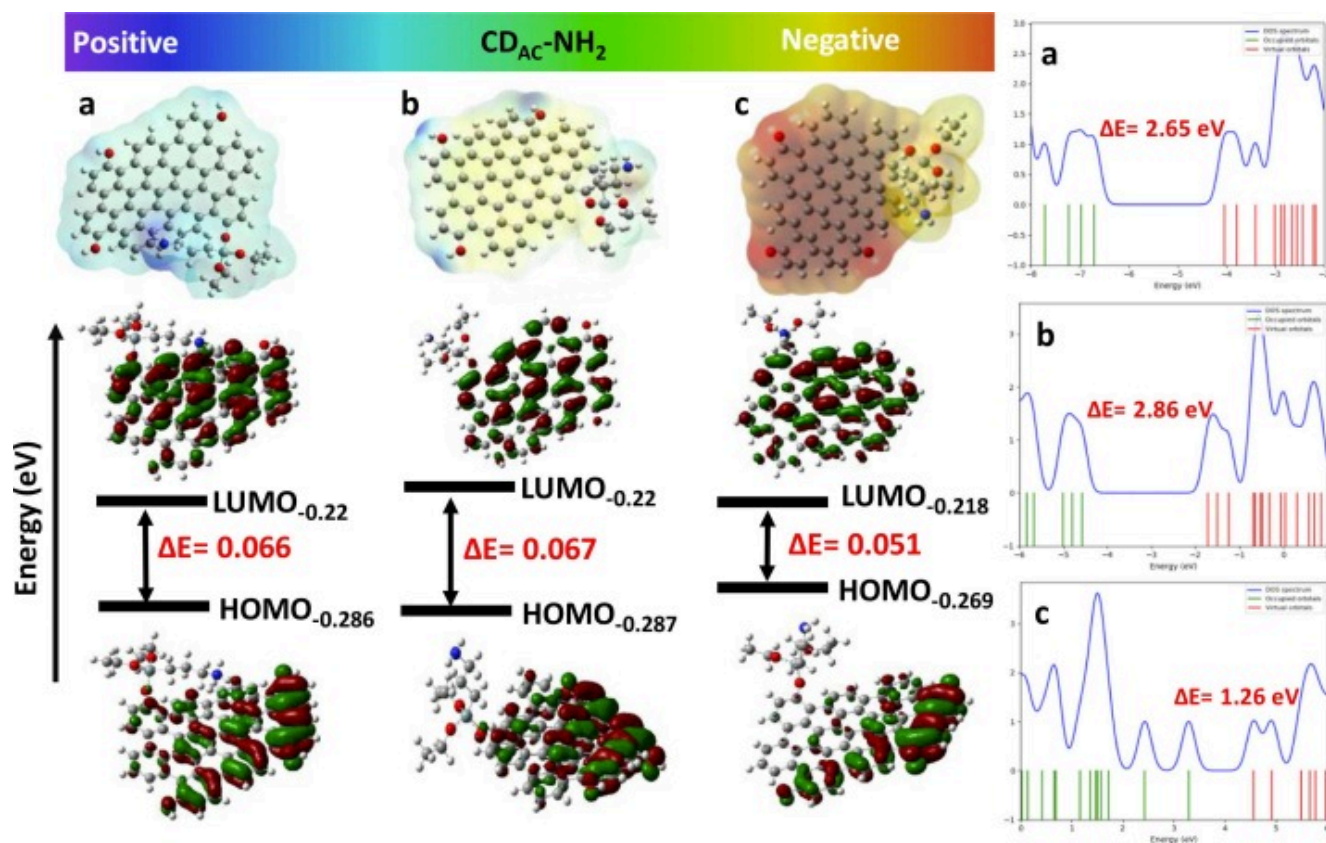
Download: Download high-res image (258KB)

Download: Download full-size image

Fig. 5. Optimized structures and $E_{ZPV}$ of $CD_{AC}$-$NH_2$ when (a) pH < 7, (b) pH = 7 and (c) pH > 7 conditions (O- ⬤, N- ⬤, Si- ⬤,C- ⬤, H- ⬤). $CD_{AC}$-$NH_2$ is stable when pH < 7.

The MEP diagrams suggest that the free -$NH_2$ group is available for further covalent modification in the case of $CD_{AC}$-$NH_2$ when pH = 7 and pH > 7 (Fig. 6). The stability of $CD_{AC}$-$NH_2$ is ascertained by the $\Delta E$ values obtained from the HOMO-LUMO gap. The uneven distribution of orbitals of these systems results in the lowering of $\Delta E$. The $\Delta E$ estimated from $CD_{AC}$-$NH_2$ when pH < 7 and pH = 7 were comparable with values ranging between 0.066–0.067 eV, and $\Delta E$ minimized to 0.051 eV when pH > 7, suggesting the system's instability. When $\Delta E$ decreases, chances for the excitation of electrons are rampant, which results in red-shifting emissions. A similar trend is observed with the $\Delta E$ calculated from the DoS spectra of $CD_{AC}$-$NH_2$ with variation in pH.
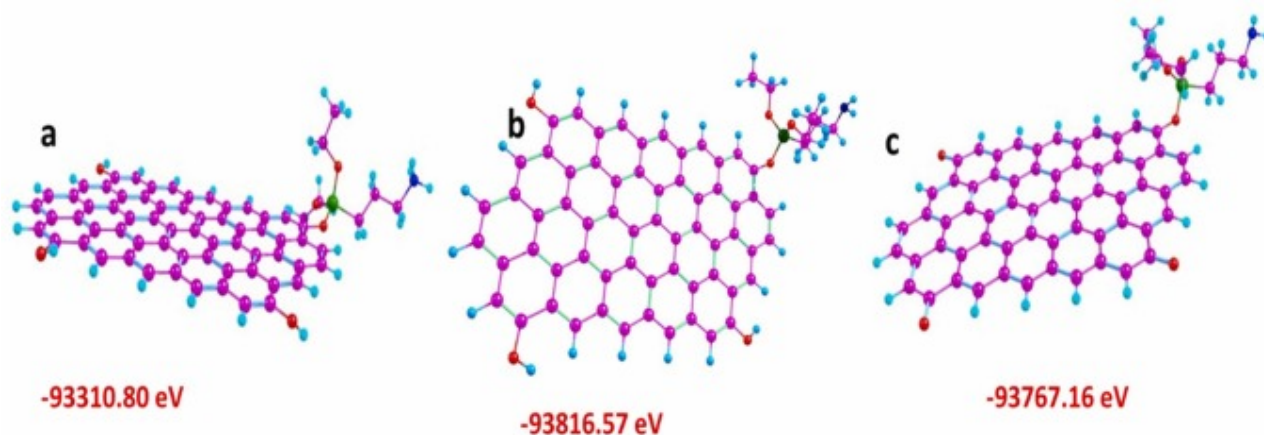
Download: Download high-res image (527KB)

Download: Download full-size image

Fig. 6. Comparison of the emission characteristics of $CD_{AC}$-$NH_2$ in (a) pH < 7, (b) pH = 7 and (c) pH > 7 conditions. $\Delta E$ is lesser when $CD_{AC}$-$NH_2$ is optimised with pH > 7.

The combined effects of APTES modification and structural orientation stabilize $CD_{ZZ}$-$NH_2$ greatly (Fig. 3), comparing their $E_{ZPV}$ with $CD_{AC}$, $CD_{ZZ}$, and $CD_{AC}$-$NH_2$. The O-Si bond length estimated when pH < 7, pH = 7, and pH > 7 in $CD_{ZZ}$-$NH_2$ are 1.68 Å, 1.68 Å and 1.65 Å, respectively, and their corresponding C-N bond length is 1.57 Å, 1.47 Å, and 1.47 Å respectively. Under pH < 7, $CD_{ZZ}$-$NH_2$ is a quaternary ammonium complex, and its $E_{ZPV}$ is much higher than the other systems(Fig. 7). The zig-zag orientation is more favourable for intermolecular HB than intramolecular. The HOMO-LUMO energy levels and the orbital diagrams in both pH < 7 and pH = 7 look similar as hardly any structural differences exist except for the change of environment around the –$NH_2$ group. Their energy levels and $\Delta E$ are thus comparable. In the pH > 7, all –OH groups are oxidized to ketones, which resulted in the alteration of the arrangement of orbitals. Hence the $\Delta E$ is reduced considerably to 0.028 eV, and red-shifted emissions are favoured (Fig. 8). The $\Delta E$ obtained from DoS spectra displays similar characteristics.

Download: Download high-res image (191KB)

Download: Download full-size image

Fig. 7. Optimized structures and $E_{ZPV}$ of $CD_{ZZ}$-$NH_2$ in (a) pH < 7, (b) pH = 7 and (c) pH > 7 conditions (O- ⬤, N- ⬤, Si- ⬤, C- ⬤, H- ⬤). $CD_{ZZ}$-$NH_2$ is stable when pH < 7.
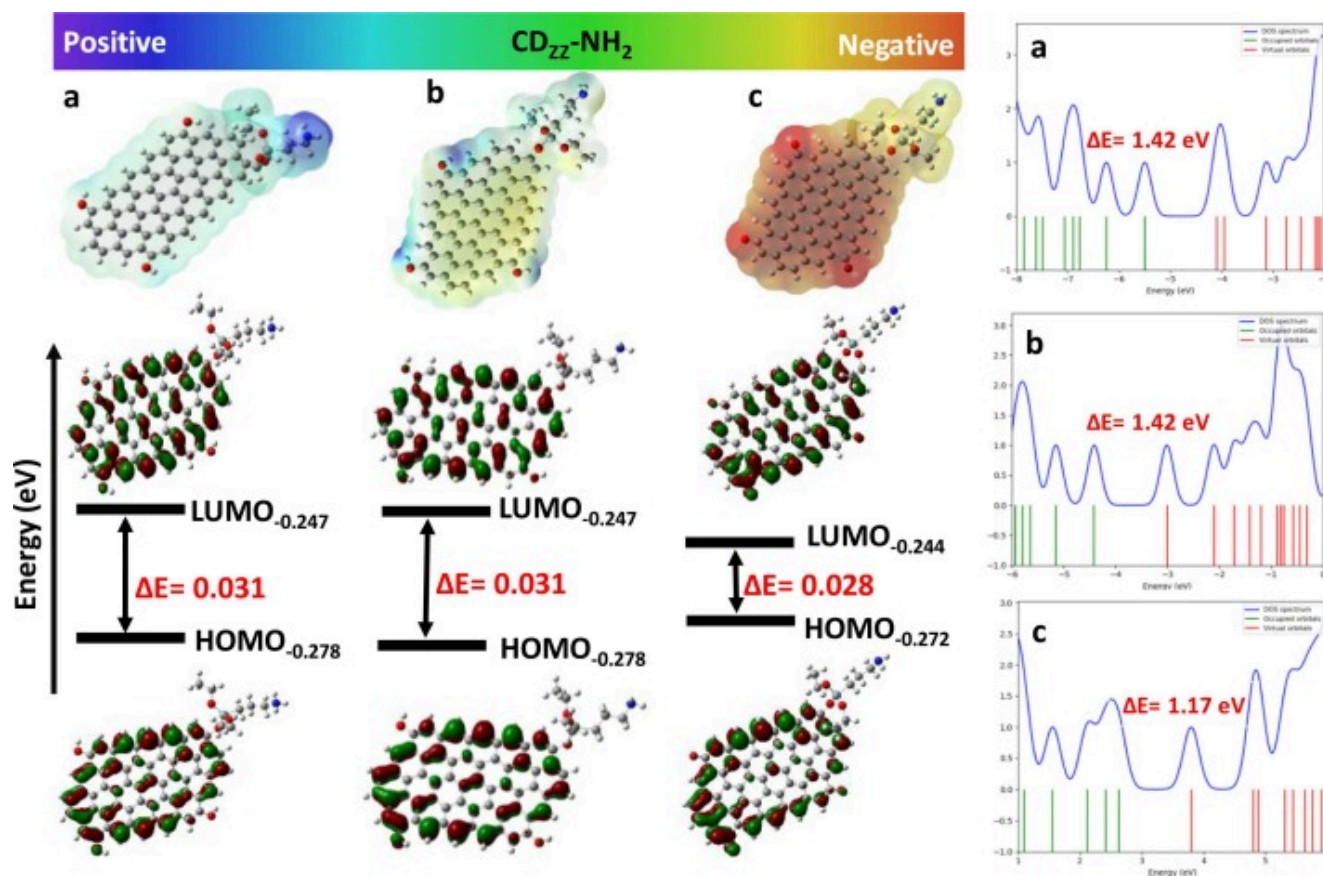


Download: Download high-res image (508KB)

Download: Download full-size image

Fig. 8. Comparison of the emission characteristics of $CD_{ZZ}$-$NH_2$ in (a) pH < 7, (b) pH = 7 and (c) pH > 7 conditions. $\Delta E$ is lesser when $CD_{ZZ}$-$NH_2$ is optimised with pH > 7.

The wavelength of maximum emission calculated from the bandgap obtained from both DoS spectra and HOMO-LUMO energy levels of the CDs discussed in this manuscript have been

tabulated in Table 1. The wavelength of emission obtained from DoS spectra ($\lambda_{(DoS)}$) for CDs with armchair orientation is closer to the experimentally observed value [24].

Table 1. Comparison of λ calculated from the ΔE obtained from DoS spectra and HOMO-LUMO energy levels.

| System | $E_{ZPV}$ (eV) | $\Delta E_{(DoS)}$ (eV) | $\Delta E_{(HOMO-LUMO)}$ (eV) | $\lambda_{(DoS)}$ (nm) | $\lambda_{(HOMO-LUMO)}$ (nm) |
|---|---|---|---|---|---|
| $CD_{AC}$ | -70,380.14 | 2.94 | 0.068 | 421.77 | 18,235.29 |
| $CD_{AC}$-$NH_2$ (pH<7) | -91784.09 | 2.65 | 0.066 | 467.92 | 18,787.88 |
| $CD_{AC}$-$NH_2$ (pH=7) | -91773.03 | 2.86 | 0.067 | 433.57 | 18,507.46 |
| $CD_{AC}$-$NH_2$ (pH>7) | -91723.94 | 1.26 | 0.051 | 984.13 | 24,313.73 |
| $CD_{ZZ}$ | -72,813.79 | 1.40 | 0.031 | 885.71 | 40,000 |
| $CD_{ZZ}$-$NH_2$ (pH<7) | -93310.80 | 1.42 | 0.031 | 873.24 | 40,000 |
| $CD_{ZZ}$-$NH_2$ (pH=7) | -93816.57 | 1.41 | 0.031 | 879.43 | 40,000 |
| $CD_{ZZ}$-$NH_2$ (pH>7) | -93767.16 | 1.17 | 0.028 | 1059.83 | 44,285.71 |

## 4. Conclusions

CDs' surface functionalization is a popular modification strategy to improve their photophysical properties. Here we attempted the theoretical interpretation (with DFT calculations) of the APTES-modification strategy adopted on CDs obtained from paper precursors, reported previously by our group. The results obtained from the APTES-modified systems ($CD_{AC}$-$NH_2$ and $CD_{ZZ}$-$NH_2$) are compared with unmodified systems ($CD_{AC}$ and $CD_{ZZ}$). $CD_{ZZ}$-$NH_2$ are more stabilized than $CD_{AC}$-$NH_2$, based on comparing their $E_{ZPV}$. The oxidation of -OH groups of CD-$NH_2$ when pH > 7 contributes to extending the conjugation of the graphitic core of CDs resulting in the enhancement of PL. The accumulation of negative charges on the surface of CD-$NH_2$ when pH > 7 implies the possibility of further modification of the CD surface. The ΔE values obtained from both DoS spectra and HOMO-LUMO analysis follow similar trends and explain the effect of pH in tuning the PL mechanism. Thus, the effect of local geometry at the terminal ends of CDs (armchair and zig-zag) and pH cannot be ignored while explaining the PL mechanism. The effect of CD sizes and the possibilities of crosslinking of APTES moieties between CD systems must be analysed further to explain the PL mechanism efficiently.

## Declaration of Competing Interest

The authors declare that they have no known competing financial interests or personal relationships that could have appeared to influence the work reported in this paper.

## Acknowledgements

## Conflict of Interest

The authors whose names are listed immediately below certify that they have NO affiliations with or involvement in any organization or entity with any financial interest (such as honoraria; educational grants; participation in speakers' bureaus; membership, employment, consultancies, stock ownership, or other equity interest; and expert testimony or patent-licensing arrangements), or non-financial interest (such as personal or professional relationships, affiliations, knowledge or beliefs) in the subject matter or materials discussed in this manuscript.

## Appendix A. Supplementary material

📄 Download: Download Word document (2MB)

Supplementary material.

.

Recommended articles

## References

[1]     X. Xu, R. Ray, Y. Gu, H.J. Ploehn, L. Gearheart, K. Raker, W.A. Scrivens
         J. Am. Chem. Soc., 126 (2004), p. 12736
         Crossref ↗    View in Scopus ↗    Google Scholar ↗

[2]     Y.P. Sun, B. Zhou, Y. Lin, W. Wang, K.A.S. Fernando, P. Pathak, M.J. Meziani, B.A. Harruff, X. Wang,
         H. Wang, P.G. Luo, H. Yang, M.E. Kose, B. Chen, L.M. Veca, S.Y. Xie
         J. Am. Chem. Soc., 128 (2006), p. 7756
         Crossref ↗    View in Scopus ↗    Google Scholar ↗

[3]     S. Nandi, S. Kolusheva, R. Malishev, A. Trachtenberg, T.P. Vinod, R. Jelinek
         Chem. - A Eur. J., 21 (2015), p. 7755
         Crossref ↗    View in Scopus ↗    Google Scholar ↗

[4]     S. Singh, R. Jelinek
         ACS Appl. Polym. Mater., 2 (2020), p. 2810
         Crossref ↗    View in Scopus ↗    Google Scholar ↗

[5]     R. Jelinek
         Carbon Nanostruct. (2017), pp. 29-46
         Crossref ↗    View in Scopus ↗    Google Scholar ↗

[6]     R. Jelinek
        Carbon Nanostruct. (2017), pp. 61-70

        Crossref ↗     View in Scopus ↗     Google Scholar ↗

[7]     G. Ayiloor Rajesh, V.L. John, A. Pookunnath Santhosh, A. Krishnan Nair Ambika, V. Thavarool
        Puthiyedath
        Part. Part. Syst. Charact., 39 (2022), 10.1002/ppsc.202200017 ↗

        Google Scholar ↗

[8]     V.L. John, A.R. Nayana, T.R. Keerthi, A.K.K. A, B.C.P. Sasidharan, V.T. P
        Macromol. Biosci. (2023), p. 2300081
        $(n/a)$

        View in Scopus ↗     Google Scholar ↗

[9]     V.L. John, T.P. Vinod
        ## Magn. Quantum Dots Bioimaging
        CRC Press,, New York (2023), pp. 71-90

        Crossref ↗     View in Scopus ↗     Google Scholar ↗

[10]    V.L. John, Y. Nair, T.P. Vinod
        Part. Part. Syst. Charact. (2021), p. 2100170
        1

        View in Scopus ↗     Google Scholar ↗

[11]    P. Anilkumar, L. Cao, J.J. Yu, K.N. Tackett, P. Wang, M.J. Meziani, Y.P. Sun
        Small, 9 (2013), p. 545

        Crossref ↗     View in Scopus ↗     Google Scholar ↗

[12]    S. Mangalath, P.S. Saneesh Babu, R.R. Nair, P.M. Manu, S. Krishna, S.A. Nair, J. Joseph
        ACS Appl. Nano Mater. (2021), 10.1021/acsanm.1c00486 ↗

        Google Scholar ↗

[13]    O. Stephan, P.M. Ajayan, C. Colliex, P. Redlich, J.M. Lambert, P. Bernier, P. Lefin
        Science, 266 (1994), p. 1683

        Crossref ↗     View in Scopus ↗     Google Scholar ↗

[14]    A.B. Bourlinos, A. Bakandritsos, A. Kouloumpis, D. Gournis, M. Krysmann, E.P. Giannelis, K.
        Polakova, K. Safarova, K. Hola, R. Zboril
        J. Mater. Chem., 22 (2012), p. 23327

        Crossref ↗     View in Scopus ↗     Google Scholar ↗

[15]    N.C.T. Martins, J. Ângelo, A.V. Girão, T. Trindade, L. Andrade, A. Mendes
        Appl. Catal. B Environ., 193 (2016), p. 67

        🗎 View PDF     View article     View in Scopus ↗     Google Scholar ↗

[16]    X.Y. Chen, Z.J. Zhang, F.F. Xu, S.Q. Shi, J.T. Zhao
        Opt. Mater. Express, 6 (2016), p. 374

Google Scholar ↗

[17] C. Xia, S. Tao, S. Zhu, Y. Song, T. Feng, Q. Zeng, J. Liu, B. Yang
Chem. - A Eur. J., 24 (2018), p. 11303

Crossref ↗     View in Scopus ↗     Google Scholar ↗

[18] C. Fan, K. Ao, P. Lv, J. Dong, D. Wang, Y. Cai, Q. Wei, Y. Xu
Nano, 13 (2018), p. 1

Google Scholar ↗

[19] P. Anilkumar, X. Wang, L. Cao, S. Sahu, J.H. Liu, P. Wang, K. Korch, K.N. Tackett, A. Parenzan, Y.P. Sun
Nanoscale, 3 (2011), p. 2023

Crossref ↗     View in Scopus ↗     Google Scholar ↗

[20] P. Das, S. Ganguly, P.P. Maity, M. Bose, S. Mondal, S. Dhara, A.K. Das, S. Banerjee, N.C. Das
J. Photochem. Photobiol. B Biol., 180 (2018), p. 56

🗎 View PDF     View article     View in Scopus ↗     Google Scholar ↗

[21] V.L. John, F.P. M, C. K P, V.T. P
Nanotechnology (2022), 10.1088/1361-6528/ac8e76 ↗

Google Scholar ↗

[22] H. Koga, T. Kitaoka, A. Isogai
J. Mater. Chem., 21 (2011), p. 9356

Crossref ↗     View in Scopus ↗     Google Scholar ↗

[23] J. Wei, J. Shen, X. Zhang, S. Guo, J. Pan, X. Hou, H. Zhang, L. Wang, B. Feng, R.S.C. Adv
3 (2013), p. 13119

Crossref ↗     View in Scopus ↗     Google Scholar ↗

[24] V. Lisa John, F. Joy, A. Jose Kollannoor, K. Joseph, Y. Nair, T.P. Vinod
J. Colloid Interface Sci., 617 (2022), p. 730

🗎 View PDF     View article     View in Scopus ↗     Google Scholar ↗

[25] S. Shokoohi, A. Arefazar, R. Khosrokhavar
J. Reinf. Plast. Compos., 27 (2008), p. 473

Crossref ↗     View in Scopus ↗     Google Scholar ↗

[26] L. Russo, F. Taraballi, C. Lupo, A. Poveda, J. Jiménez-Barbero, M. Sandri, A. Tampieri, F. Nicotra, L. Cipolla
Interface Focus, 4 (2014), p. 20130040

Crossref ↗     View in Scopus ↗     Google Scholar ↗

[27] Y. Xie, C.A.S. Hill, Z. Xiao, H. Militz, C. Mai
Compos. Part A Appl. Sci. Manuf., 41 (2010), p. 806

🗎 View PDF     View article     View in Scopus ↗     Google Scholar ↗

[28] B. Wang, J. Yu, L. Sui, S. Zhu, Z. Tang, B. Yang, S. Lu

Adv. Sci., 8 (2021), p. 1

Google Scholar ↗

[29]   M.A. Sk, A. Ananthanarayanan, L. Huang, K.H. Lim, P. Chen
       J. Mater. Chem. C., 2 (2014), p. 6954

       View in Scopus ↗     Google Scholar ↗

[30]   M.J. Frisch
       (2009)
         ⟨http//www.gaussian.com/⟩ ↗

       Google Scholar ↗

[31]   S. Miertuš, E. Scrocco, J. Tomasi
       Chem. Phys., 55 (1981), p. 117

       📄 View PDF     View article     View in Scopus ↗     Google Scholar ↗

[32]   R. Dennington, T.A. Keith, J.M. Millam, 2019.

       Google Scholar ↗

[33]   "Chemcraft - graphical software for visualization of quantum chemistry computations,"
       can be found under ⟨https://www.chemcraftprog.com/citation.html⟩ ↗, n.d.

       Google Scholar ↗

[34]   M. Zhao, F. Yang, Y. Xue, D. Xiao, Y. Guo
       ChemPhysChem, 15 (2014), p. 950

       Crossref ↗     View in Scopus ↗     Google Scholar ↗

[35]   A.D. Becke
       J. Chem. Phys., 98 (1993), p. 5648

       View in Scopus ↗     Google Scholar ↗

[36]   C. Lee, W. Yang, R.G. Parr
       Phys. Rev. B, 37 (1988), p. 785

       View in Scopus ↗     Google Scholar ↗

[37]   V.A. Rassolov, J.A. Pople, M.A. Ratner, T.L. Windus
       J. Chem. Phys., 109 (1998), p. 1223

       View in Scopus ↗     Google Scholar ↗

[38]   E.D. Glendening, C.R. Landis, F. Weinhold
       J. Comput. Chem., 34 (2013), p. 1429

       Crossref ↗     View in Scopus ↗     Google Scholar ↗

[39]   N.M. O'boyle, A.L. Tenderholt, K.M. Langner
       J. Comput. Chem., 29 (2008), p. 839

       Crossref ↗     Google Scholar ↗

[40]   R. Ghafouri, F. Ektefa, M. Zahedi

Nano, 10 (2015), p. 1

Crossref ↗    Google Scholar ↗

[41]  K. Wolinski, J.F. Hinton, P. Pulay
J. Am. Chem. Soc., 112 (1990), p. 8251

Crossref ↗    View in Scopus ↗    Google Scholar ↗

[42]  P. Pulay, J.F. Hinton
Encycl. Magn. Reson. (2007), p. 1

Google Scholar ↗

[43]  R.A. Klein
Chem. Phys. Lett., 425 (2006), p. 128

📄 View PDF    View article    View in Scopus ↗    Google Scholar ↗

[44]  P.M. Fasila, A. Rahana, A.R. Biju
Comput. Theor. Chem., 1205 (2021), Article 113425

📄 View PDF    View article    View in Scopus ↗    Google Scholar ↗

[45]  R. Ameen, P.M. Fasila, A.R. Biju
Comput. Theor. Chem., 1203 (2021), Article 113346

📄 View PDF    View article    View in Scopus ↗    Google Scholar ↗

[46]  G.A. Jeffrey
An Introduction to Hydrogen Bonding
Oxford University Press,, New York (1997)

Google Scholar ↗

[47]  Y. Nair, F. Joy, T.P. Vinod, M.C. Vineetha, M.R.P. Kurup, S. Kaya
Mol. Divers. (2023), 10.1007/s11030-023-10599-6 ↗

Google Scholar ↗

[48]  L. Pauling
J. Am. Chem. Soc., 53 (1931), p. 1367

Crossref ↗    View in Scopus ↗    Google Scholar ↗

[49]  J.C. Slater
Phys. Rev., 37 (1931), p. 481

View in Scopus ↗    Google Scholar ↗

[50]  C.A. Charles, A. Coulson
1910-1974
Valence / by C.A. Coulson, Oxford University Press,, London; New York (1961)

Google Scholar ↗

[51]  J.P. Foster, F. Weinhold
J. Am. Chem. Soc., 102 (1980), p. 7211

Crossref ↗    View in Scopus ↗    Google Scholar ↗

[52]   F. Weinhold, C.R. Landis, A.E. Reed, F. Weinhold

Chem. Educ. Res. Pr., 2 (2001), p. 91

Google Scholar ↗

[53]   T. Enoki, S. Fujii, K. Takai

Carbon N. Y, 50 (2011), p. 3141

Google Scholar ↗

[54]   H. Ohsaki, K. Miura, A. Imai, M. Tada, M.A. Aegerter

J. Sol. -Gel Sci. Technol., 2 (1994), p. 245

View in Scopus ↗     Google Scholar ↗

[55]   J.J. Gutiérrez Moreno, K. Pan, Y. Wang, W. Li

Langmuir, 36 (2020), p. 5680

Crossref ↗     View in Scopus ↗     Google Scholar ↗

## Cited by (0)

We attempt to explain the photoluminescence (PL) mechanism of APTES-modified carbon dots (CDs) utilizing DFT calculations, which is the first of its kind. Hydrogen bonding interactions are analyzed to explain the structural stability of the APTES-modified CDs. The pH and local geometry around the edges (armchair and zig-zag orientations) play a pivotal role in modulating the PL of APTES-modified CDs, thereby improving their quantum yield (QY). Such improved QYs of APTES-modified CDs enable their optoelectronic utilities.

ELSEVIER

ℝ RELX™